Simulating surface tension with smoothed particle hydrodynamics

Joseph P. Morris*

School of Civil Engineering, Purdue University, West Lafayette, IN 47907, U.S.A.

SUMMARY

A method for simulating two-phase flows including surface tension is presented. The approach is based upon smoothed particle hydrodynamics (SPH). The fully Lagrangian nature of SPH maintains sharp fluid–fluid interfaces without employing high-order advection schemes or explicit interface reconstruction. Several possible implementations of surface tension force are suggested and compared. The numerical stability of the method is investigated and optimal choices for numerical parameters are identified. Comparisons with a grid-based volume of fluid method for two-dimensional flows are excellent. The methods presented here apply to problems involving interfaces of arbitrary shape undergoing fragmentation and coalescence within a two-phase system and readily extend to three-dimensional problems. Boundary conditions at a solid surface, high viscosity and density ratios, and the simulation of free-surface flows are not addressed. Copyright © 2000 John Wiley & Sons, Ltd.

KEY WORDS: interfacial flow; meshless methods; surface tension

1. INTRODUCTION

Surface tension forces play an important role in many systems within both natural and artificial environments. For example, applications in food processing, cosmetics, metal casting, enamelling, fuel injection systems, and sub-surface contaminant transport all involve effects resulting from the tension present at liquid–liquid interfaces. Many techniques have been developed to simulate multiphase flows with surface tension. Some of these use simplifying assumptions to increase computational efficiency, making it difficult to include extra physical or chemical effects or complicated boundary conditions. In addition, it can be difficult to extend some methods to three-dimensional problems. Smoothed particle hydrodynamics (SPH) is a computational technique originally developed to model astrophysical problems [1,2], however, it has since been extended to model a wide variety of problems in computational physics [3–5]. SPH is a fully Lagrangian technique where fluid interfaces are advected with

* Correspondence to: Geophysics and Global Security Division, Lawrence Livermore National Laboratory, PO Box 808, L-206, Livermore, CA 94551-9900, U.S.A. Tel.: +1 925 4244581.

very little numerical diffusion. The SPH formalism readily accommodates extra physical and chemical effects and highly irregular, mobile or even deformable boundaries [6,7]. This flexibility readily carries over into three-dimensional problems. However, SPH can often be more computationally expensive than competing methods for idealized problems. The extension of SPH to model low Reynolds number incompressible flows has only recently been achieved [7–9]. Some theoretical work has been done towards incorporating surface tension effects into SPH [10,11], however, this work is one of the first to present successful simulations. In this work we simulate surface tension acting at an interface between two fluids of the same density and viscosity. The methods presented can be readily applied to problems involving fluids of similar density and viscosity. The extension of the method to higher density and viscosity ratios (e.g. at an air–water interface) is not considered.

2. INTERFACE TRACKING TECHNIQUES

A flexible fluid dynamics technique that accounts for surface tension must be able to handle arbitrarily shaped interfaces between immiscible fluids. Many techniques have been developed to model fluid–fluid interfaces [12–19] (see Scardovelli and Zaleski [20] for a recent review), however, few are able to simulate general geometries. The more restricted methods model the behaviour of isolated globules and cannot follow coalescence or fragmentation. In the case of immiscible fluids, each corresponding to a different 'colour', c, interface tracking can be achieved by simulating the advection of the colour function

$$\frac{\partial c}{\partial t} + \mathbf{v} \cdot \nabla c = 0 \tag{1}$$

Many other types of discontinuities, such as shocks, involve an underlying mechanism that serves to limit numerical diffusion. The techniques developed to simulate advection of contact discontinuities involve special features, which seek to maintain sharp interfaces. Rider and Kothe [17] and Rudman [19] review some of these approaches.

High-order advection techniques, typically developed for compressible flows, track discontinuities with high accuracy and very little broadening (e.g. flux corrected transport (FCT) [19] and the piecewise parabolic method (PPM) [21]). Such methods can be used to advect the colour function through the computational domain and thus track the material interface [17,19]. Despite the relatively low numerical diffusion present in such schemes, interfaces are smoothed out over long periods and flow features can be lost [17].

Level set methods have been successfully applied to problems in geometry, image processing, materials science, and fluid flow [22]. Typically in fluid problems, the interface is defined to be the zero level set of a distance function (ϕ) from the interface [22,23]. The distance function itself is advected using low diffusion advection schemes and the colour function is then defined in terms of the value of the distance function. This approach ensures very sharp interfaces, however, exact conservation of mass is not guaranteed.

Some techniques geometrically reconstruct the interface at each time step to maintain sharp interfaces. For example, the simplified line interface calculation (SLIC) method [24] uses a

straightforward algorithm to guarantee sharp interfaces. However, the reconstruction of the fluid–fluid interface results in artificial ejection of fluid globules. The volume of fluid (VOF) method [25], and the method of Youngs [26] use more sophisticated reconstruction algorithms to ensure sharp interfaces. The reconstruction process can cause small globules of fluid to prematurely pinch off in the presence of strong vorticity or when flow features approach the grid size [17]. Nevertheless, these methods provide a robust approach to maintaining sharp interfaces using an Eulerian mesh.

The colour function may be evolved in a Lagrangian fashion by assigning fluid characteristics to 'particles' or 'markers', which are then advected through the computational domain. In general, this may be achieved using particles on the interface alone (surface-marker methods) or by employing particles which fill the entire computational domain (volume-marker methods). Surface-markers have been used extensively to track the location of interfaces with high accuracy [27–29]. Volume-marker methods use markers throughout the computational domain to track different phases. This approach may be exploited by fully Lagrangian techniques (such as SPH in this work) or by methods that employ both a grid and particles [30]. These methods maintain interfaces of constant width, proportional to the numerical resolution employed. While volume particle methods (such as SPH) can provide excellent interface tracking capabilities [17,30], they are typically more computationally expensive for a given resolution. Furthermore, the motion of the particles may lead to the formation of features smaller than the resolution of the method. For example, very thin filaments of fluid may form which may only be spanned by one or two particles, at which point calculations of pressure gradients and surface tension will become inaccurate. Nevertheless, the SPH formalism is versatile and can be readily extended to include extra physical and chemical effects. In addition, SPH has been shown to readily model complicated and dynamic boundaries [6,7]. The presence of solid boundaries of arbitrary shape can hinder the implementation of other techniques. Furthermore, many front-tracking techniques become excessively complicated or break down completely when more than two fluid phases are considered. With SPH, each extra phase is modelled simply by introducing an extra 'species' of particle.

3. THE CONTINUUM SURFACE FORCE METHOD

The continuum surface force (CSF) method [31] permits numerical simulation of surface tension without placing restrictions upon the flow geometry. It has been applied successfully to many problems, including low gravity flows [31,32] and liquid–liquid jets [33]. The CSF approach models processes localized to a fluid interface by applying them to fluid elements in the transition region of the interface. Interfacial phenomena, such as surface tension and phase change, are translated into volume processes having a net effect that emulates the desired physics. This approach can be regarded as an immersed interface method [34].

In the CSF model, surface tension is translated into a force per unit volume, $\mathbf{F}_s$, by

$$\mathbf{F}_s = \mathbf{f}_s \delta_s \tag{2}$$

where δ_s is a normalized function (the surface delta function), which peaks at the interface and $\mathbf{f}_s$ is the force per unit area given by

$$\mathbf{f}_s = \sigma \kappa \hat{\mathbf{n}} + \nabla_s \sigma \tag{3}$$

where σ is the surface tension coefficient, $\hat{\mathbf{n}}$ is the unit normal to the interface, κ is the curvature of the interface and ∇_s is the surface gradient. The second term in (3) acts tangentially to the interface, forcing fluid from regions of low surface tension to higher surface tension. In this work, surface tension is assumed constant throughout the fluid and the surface gradient term is neglected. The first term in (3) is a force acting normal to the interface corresponding to the net surface tension force due to the local curvature. This force acts to smooth regions of high curvature, in an attempt to reduce the total surface area (and hence surface energy).

The normal in (3) can be obtained using

$$\mathbf{n} = \frac{\nabla c}{[c]} \tag{4}$$

where c is the colour function identifying each fluid in the problem and $[c]$ is the jump in c across the interface. The curvature can be calculated using [35]

$$\kappa = -\nabla \cdot \hat{\mathbf{n}} \tag{5}$$

There are many possible choices for δ_s, however, it should be normalized such that its integral through the boundary is one. This is necessary for the correct physics of the interface to be recovered as the resolution is increased. The function should also be non-zero only in those fluid elements that correspond to the transition regions in the numerical method. The surface delta function employed in this work is [31]

$$\delta_s = |\mathbf{n}| \tag{6}$$

4. THE SPH EQUATIONS

Using SPH, the fluid is represented by particles, typically of fixed mass, which follow the fluid motion, advect contact discontinuities, preserve Galilean invariance, and reduce computational diffusion of various properties including momentum. The equations governing the evolution of the fluid become expressions for interparticle forces and fluxes when written in SPH form. Using the standard approach to SPH [3,4], the particles (which may also be regarded as interpolation points) move with the local fluid velocity. Each particle carries mass m, velocity $\mathbf{v}$, and other fluid quantities specific to a given problem. The equations governing the evolution of fluid quantities are expressed as summation interpolants using a kernel function W with smoothing length h. For example, the density at particle a, ρ_a, may be evaluated using

$$\rho_a = \sum_b m_b W_{ab} \tag{7}$$

where W_{ab} denotes

$$W_{ab} = W(\mathbf{r}_{ab}, h) \tag{8}$$

and

$$\mathbf{r}_{ab} = \mathbf{r}_a - \mathbf{r}_b \tag{9}$$

where $\mathbf{r}_a$ denotes the position of particle a. The kernel typically takes the form

$$W(\mathbf{r}_{ab}, h) = \frac{1}{h^{\mathscr{N}}} f\left(\frac{|\mathbf{r}_{ab}|}{h}\right) \tag{10}$$

where $\mathscr{N}$ is the number of dimensions and the function f is typically either a Gaussian or a spline approximating a Gaussian [36]. Typically, the smoothing length h is taken to be $1-1.5$ times the average particle separation.

Other expressions for quantities at the particles are obtained by summation involving the kernel or its derivatives. For example, the SPH expression for the pressure gradient term used in this work is

$$-\left(\frac{1}{\rho}\nabla p\right)_a = -\sum_b m_b\left(\frac{p_a + p_b}{\rho_a \rho_b}\right)\nabla_a W_{ab} \tag{11}$$

where p_a is the pressure at particle a and ∇_a denotes the gradient with respect to the co-ordinates of particle a. For a kernel of the form in (10), this pressure gradient formulation conserves momentum exactly, since forces acting between individual particles are antisymmetric.

Most grid-based techniques treat the flow of water as incompressible since the speed of sound in water is usually large compared with bulk fluid motions (i.e. a very low Mach number). Using SPH, pressure is an explicit function of local fluid density and it is most natural to use a quasi-incompressible equation of state [6]. Since the actual equation of state for water would require a prohibitively small time step for stability (by the Courant–Friedrich–Lewy (CFL) condition [37]), an artificial state equation is used. This work uses

$$p = c_s^2(\rho_a - \rho_0) \tag{12}$$

where ρ_0 is the reference density of the fluid and c_s is the speed of sound. Subtracting the reference density was found to lead to more accurate simulations. The most probable reason for this is that subtracting the reference density removes a zeroth-order error term associated with conservative forms of SPH pressure gradients [38]. The chosen sound speed is low enough to be practical, yet high enough to restrict density fluctuations within the desired limits

(typically about 1 per cent [6]). For example, Morris *et al*. [7] suggested that c_s be comparable with the largest of

$$c_s^2 \sim \frac{V^2}{\Delta}, \frac{\mu V}{\rho L \Delta}, \frac{aL}{\Delta} \tag{13}$$

where Δ is the desired relative variation in density, and V, L and a are typical velocity, length and body acceleration scales, and μ is the dynamic viscosity.

Viscous forces were calculated using a formulation recently applied to low Reynolds number flow [7]. The SPH momentum equation, may then be written [7]

$$\frac{d\mathbf{v}_a}{dt} = -\sum_b m_b \frac{p_a + p_b}{\rho_a \rho_b} \nabla_a W_{ab} + \sum_b \frac{m_b (\mu_a + \mu_b)\mathbf{v}_{ab}}{\rho_a \rho_b} \left(\frac{1}{r_{ab}} \frac{\partial W_{ab}}{\partial r_a} \right) + (\mathbf{a}_s)_a \tag{14}$$

where $\mathbf{a}_s$ denotes the surface tension force per unit mass.

5. CALCULATING INTERFACIAL CURVATURE WITH SPH

In order to obtain realistic estimates of surface tension using (3), the curvature κ must be calculated accurately. This requires the accurate estimation of the surface normals and their divergence.

The simplest SPH expression for $\mathbf{n}$ is given by

$$\mathbf{n}_a = \sum_b \frac{m_b}{\rho_b} c_b^i \nabla_a W_{ab} \tag{15}$$

where c_b^i is the colour index of particle b. This expression was used by Monaghan [11] to derive an SPH surface tension force expression using variational principles.

More accurate estimates of the surface normal are obtained when the colour field is smoothed by convolution with a high order kernel [39,40]. With SPH this smoothing is naturally achieved by using the standard interpolation expression

$$c_a = \sum_b \frac{m_b}{\rho_b} c_b^i W_{ab} \tag{16}$$

Additional improvements in accuracy are obtained by using

$$\mathbf{n}_a = \sum_b \frac{m_b}{\rho_b} (c_b - c_a) \nabla_a W_{ab} \tag{17}$$

since this involves a difference between neighbouring particle colours.

The simplest SPH expression for the divergence of $\hat{\mathbf{n}}$ is

$$(\nabla \cdot \hat{\mathbf{n}})_a = \sum_b \frac{m_b}{\rho_b} \, \hat{\mathbf{n}}_b \cdot \nabla_a W_{ab} \tag{18}$$

however, a more accurate estimation of divergence is obtained using [4]

$$(\nabla \cdot \hat{\mathbf{n}})_a = \sum_b \frac{m_b}{\rho_b} (\hat{\mathbf{n}}_b - \hat{\mathbf{n}}_a) \cdot \nabla_a W_{ab} \tag{19}$$

Unfortunately, if Equations (19) and (17) are used to evaluate curvature, large errors will occur at the fringes of the transition zone. The main difficulty is that the calculation of curvature requires the normalized normals $\hat{\mathbf{n}}$. Some distance away from the interface, $\mathbf{n}$ will be small and may have an erroneous direction. As a result, any estimate of curvature that uses these normals will be inaccurate. For example, Figure 1 shows the curvature calculated for a circle of radius 0.25 in the neighbourhood of a line through its centre. The correct curvature as a function of distance is represented by the solid line. The SPH particles were placed on a hexagonal lattice of spacing 0.01, and a quintic spline kernel with smoothing length of 1.5 times the nearest neighbour distance was used. The estimated curvature passes through the exact result near the interface, but has a wide scatter near the fringes of the smoothed interface. The actual extremes in the estimate of curvature are approximately -50 and 50. In a dynamic simulation, these errors rapidly disrupt the interface.

A more accurate curvature estimate is obtained by using appropriate criteria to determine if a normal is 'reliable' before including it in a divergence calculation. For this work, the following were used:
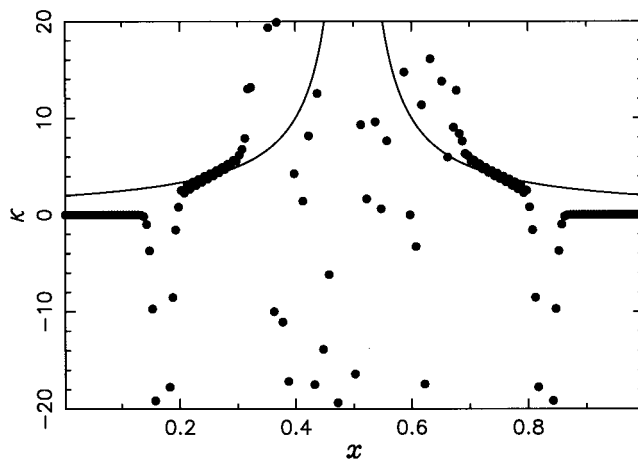

Figure 1. Curvature for a circle of radius 0.25 centred at $x = 0.5$, $y = 0.5$. Solid circles are the SPH estimates of curvature using all normals (Equations (17) and (19)). The solid line gives the correct curvature ($\kappa = 1/r$).

$$N_a = \begin{cases} 1, & \text{if } |\mathbf{n}_a| > \epsilon \\ 0, & \text{otherwise} \end{cases} \tag{20}$$

and

$$\hat{\mathbf{n}}_a = \begin{cases} \mathbf{n}_a/|\mathbf{n}_a|, & \text{if } N_a = 1 \\ 0, & \text{otherwise} \end{cases} \tag{21}$$

Typically, ϵ was taken to be $0.01/h$ in this study, since this scales appropriately with the resolution length and is proportional to the maximum gradient of c achievable for a given smoothing length. It is then necessary to correct (19) for the absence of normals in the neighbourhood of particle a. This can be done by defining an intermediate estimate of divergence using a sum over reliable neighbouring normals

$$(\nabla \cdot \hat{\mathbf{n}})_a^* = \sum_b \min(N_a, N_b) \frac{m_b}{\rho_b} (\hat{\mathbf{n}}_b - \hat{\mathbf{n}}_a) \cdot \nabla_a W_{ab} \tag{22}$$

This initial estimate can be corrected by a factor $\mathscr{C}_a$,

$$(\nabla \cdot \hat{\mathbf{n}})_a = (\nabla \cdot \hat{\mathbf{n}})_a^* / \mathscr{C}_a \tag{23}$$

where

$$\mathscr{C}_a = \sum_b \min(N_a, N_b) \frac{m_b}{\rho_b} W_{ab} \tag{24}$$

reflects the local number density of particles with 'reliable' estimations of normals. Similar approaches have been used previously to improve the accuracy of first derivatives [5,38] and can be derived within the formalism of element free Galerkin methods [41]. Results using this approach are shown in Figure 2. The modified SPH estimates of curvature are very close to the exact result, and no scatter at the fringes of the interface is evident.

The surface tension force can now be included in (14) using

$$(\mathbf{a}_s)_a = -\frac{\sigma_b}{\rho_a} (\nabla \cdot \hat{\mathbf{n}})_a \mathbf{n}_a \tag{25}$$

The incorporation of surface tension places an additional restriction upon the sound speed of the SPH fluid. For a static cylinder, the pressure jump across the interface satisfies

$$\delta p = \sigma \kappa \tag{26}$$

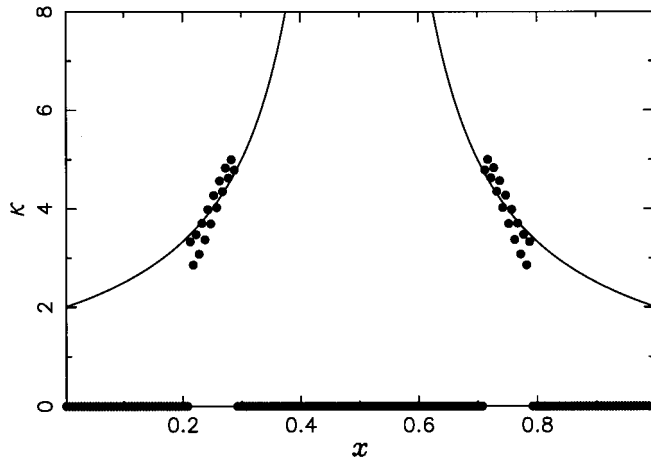thus, the sound speed squared should be comparable with

Figure 2. Curvature for a circle of radius 0.25 centred at $x = 0.5$, $y = 0.5$. Solid circles are the SPH estimates of curvature using only the 'reliable' normals (Equations (22) and (23)). The solid line gives the correct curvature ($\kappa = 1/r$).

$$c_s^2 \sim \frac{\sigma \mathcal{K}}{\rho_0 \Delta} \tag{27}$$

where $\mathcal{K}$ is the typical curvature. To maintain numerical stability with respect to surface tension forces when using explicit time integration, this work uses a CFL condition [37] based upon the capillary wave phase velocity, similar to that suggested by Brackbill et al. [31]

$$\Delta t_s \leq 0.25 \left[\frac{\bar{\rho} h^3}{2\pi\sigma} \right]^{1/2} \tag{28}$$

In addition, conditions due to the sound waves in the SPH fluid,

$$\Delta t \leq 0.25 \frac{h}{c_s} \tag{29}$$

the magnitude of individual particle accelerations, a, (see Monaghan [4]),

$$\Delta t \leq 0.25 \min_b \left(\frac{h}{a_b} \right)^{1/2} \tag{30}$$

and viscous diffusion,

$$\Delta t \leq 0.125 \frac{\rho h^2}{\mu} \tag{31}$$

must be satisfied [7].

6. A MOMENTUM CONSERVING FORM

The method presented above does not guarantee exact conservation of linear or angular momenta. There are several approaches that can be employed to derive expressions for conservative forces. For example, Lafaurie *et al.* [42] derived a surface tension force expressed as the gradient of a tensor

$$\kappa \hat{\mathbf{n}} \delta_s = \nabla[(\mathbf{I} - \hat{\mathbf{n}} \times \hat{\mathbf{n}}) \delta_s] \tag{32}$$

A suitable SPH approximation for this may be written as

$$(\mathbf{a}_s)_a = \left(\frac{1}{\rho} \frac{\partial \mathscr{S}_{ij}}{\partial x_j} \right)_a = \sum_b m_b \frac{(\mathscr{S}_{ij})_a + (\mathscr{S}_{ij})_b}{\rho_a \rho_b} \nabla_{a,j} W_{ab} \tag{33}$$

where

$$\mathscr{S}_{ij} = \delta_s (\delta_{ij} - \hat{\mathbf{n}}_i \hat{\mathbf{n}}_j) \tag{34}$$

Here, δ_{ij} denotes the Kronecker delta, $\nabla_{a,j} W_{ab}$ is the jth component of the gradient of W_{ab} with respect to $\mathbf{r}_a$, and repetition of the j index implies summation. To improve accuracy, only normals satisfying (20) are included. Since the reciprocal particle contributions in (33) are antisymmetric, linear momentum is conserved. There are several potential disadvantages to this approach. Since this formulation no longer involves a direct calculation of curvature, it is more difficult to exploit a 'correction factor' such as that introduced in Section 5. In addition, this method is potentially unstable. It is well known that SPH particles are unstable to attractive forces when momentum conserving formulations are used [38,43–47]. The effect of the $\delta_s \mathbf{I}$ term in (32) is a tension. The net force between particles, however, will remain repulsive provided the pressure force dominates

$$p > \sigma \max \delta_s \tag{35}$$

As the resolution is increased, the maximum of δ_s will increase and at some point, the method will become unstable. The simplest solution to this problem is to replace $\mathscr{S}_{ij}$ with a modified tensor

$$\mathscr{S}_{ij}^* = \mathscr{S}_{ij} - \delta_{ij} \max \delta_s \tag{36}$$

This avoids tension occurring between particles and results in a stable solution for the test problems. A similar approach has been used to stabilize SPH simulations of magnetohydrodynamics [38,44]. However, it has also been established that excessive 'over pressure' acting between SPH particles can lead to long wavelength instabilities [38,45,47]. Such problems were not observed for the test results considered here, however, as resolution is increased the peak value of δ_s will increase and this particular instability may become significant. More

sophisticated methods for stabilizing SPH particles in tension have been developed [5], and may be less susceptible to this problem.

It is also possible to derive formulations that exactly conserve linear and angular momenta using a Lagrangian. The approach permits us to take an SPH expression for the surface energy resulting from surface tension and transform it into an equation of motion. For example, Monaghan [11] considered the surface energy at a free surface of SPH particles. However, these formulations involve explicit second derivatives of the kernel, which (for lower order spline kernels) tend to be inaccurate [48]. It is also more difficult to relate the stability properties of these formulations to the established stability properties of SPH [38,43–47].

7. REMOVING THE SINGULARITY

One disadvantage of the formulations presented above is that δ_s introduces a singularity into the solution for the pressure field as the resolution is increased. Sussman *et al.* [49] suggested substituting (6) (taking $[c] = 1$) into (2) and re-writing as

$$\mathbf{F}_s = \sigma\kappa\nabla c = \nabla(\sigma\kappa c) - \sigma c\nabla\kappa \tag{37}$$

This assumes that κ is defined throughout the solution domain. This can be done in several ways by smoothly interpolating κ from the interface into regions where it was not initially defined. The first term of (37) can now be incorporated into the pressure term of the momentum equations by introducing new definitions for the pressure and surface tension force

$$p^* = p - \sigma\kappa c \tag{38}$$

$$\mathbf{F}_s^* = -\sigma c\nabla\kappa \tag{39}$$

Thus, the same momentum equation (14) can be used with (39) replacing the surface tension force and with modified pressure boundary conditions which accommodate the new definition of pressure. The volumetric force (39) no longer contains a delta function as resolution is increased, improving the numerical solution for the pressure field. This approach has been used by Rider *et al.* [50] to permit the simulation of the nozzle of an ink jet printer.

The other implementations of surface tension weighted particles within the interface more heavily than particles outside the interface. The new approach weights all particles according to their colour only. Consequently, erroneous estimates of κ may be extrapolated throughout the computational domain, potentially disrupting the solution. Under the original definition of the surface tension force, less reliable estimates of curvature on the fringes of the interface received a lower weighting. To improve the stability of this technique, only the curvatures of particles satisfying $|\mathbf{n}_a| > \epsilon_2$ were used. The same ϵ as before was used to decide which normals were included in the calculation of curvature. The second, larger ϵ_2 was used to decide which particles had reliable estimates of local curvature. Curvatures satisfying this condition were then extrapolated throughout the domain.

It is expected that this method will exhibit better numerical stability properties as the resolution is increased. However, the evaluation of the gradient of the curvature field requires an extra pass over all the particles and a corresponding increase in computational effort.

8. TEST CASES

In the following sections, the performances of the methods presented are investigated. For brevity, the approaches are denoted

- **Method I** uses a force based directly on the interfacial curvature (25).
- **Method II** uses the momentum conserving form described in Section 6.
- **Method III** employs the gradient of the curvature as described in Section 7.

8.1. Stability of an interface

Previous studies using the CSF formulation have reported a numerical instability which develops at the fluid–fluid interface [40,42]. This instability leads to non-zero velocities at the interface, termed parasitic currents, causing unrealistic fluxes across the interface between two fluids. Using SPH these parasitic currents could lead to particle disorder at the fluid–fluid boundary, having the effect of diffusing the interface.

In order to study the significance of this phenomenon for the methods presented here, a simple static test case was considered. A periodic domain spanning 0.5 units in the x-direction and 1 unit in the y-direction, with the upper half filled with fluid of colour 1 and the lower half with colour 0 was simulated. The fluid densities were 1, the surface tension coefficient was 1, and no viscous forces were included. The sound speed of the fluid was set to be approximately 20 in the simulation units. At $t = 0$, a random velocity field was imposed with kinetic energy approximately six orders of magnitude less than the internal energy of the fluid. The ratio of kinetic energy to the internal energy of the fluid was recorded as a function of time for each method for several combinations of smoothing lengths.

It is well established that the stability properties of SPH improve when smoother kernels, more closely resembling a Gaussian are employed [38,45,47]. The simulations presented here used cubic and quintic spline approximations to a Gaussian kernel [7]. The use of different levels of smoothing to evaluate the curvature and the surface delta function (here denoted by h_0 and h_1 respectively) was also considered. In this way, by using a slightly larger smoothing length for curvature calculation, more reliable estimates of curvature are obtained in the region where the surface normals (obtained using h_1) are non-zero. Grid-based implementations of the CSF method have achieved a similar result by using a wide stencil for the curvature estimate [30,31]. One disadvantage of this approach is that the computational effort for each time step increases as h_0 is increased and the time step size must decrease as h_1 is decreased to ensure stability of the time integration. Consequently, for a given level of resolution, employing two smoothing lengths can be significantly more computationally intensive.

Figure 3 compares the evolution of kinetic energy using Method I for several choices of kernel and smoothing length. It is seen that, for the same parameters, the quintic spline is consistently more stable than the cubic spline. In addition, as the smoothing length is increased
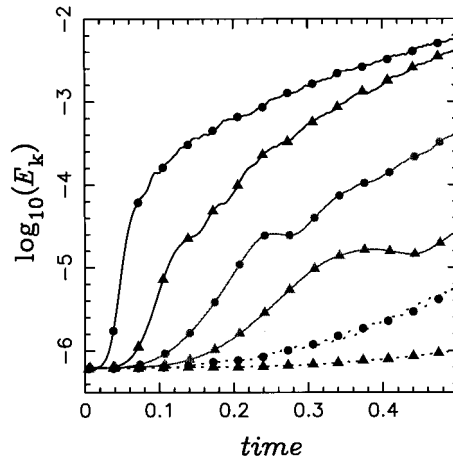
Figure 3. Evolution of $\log_{10} E_k$ with time for Method I. Curves marked with circles and triangles denote use of the cubic and quintic splines respectively. Use of $h_0 = h_1 = 1.0$, $h_0 = h_1 = 1.5$ and $h_0 = 1.5$, $h_1 = 1.0$ are denoted by black, mid-grey and dotted curves respectively.

from $h = 1$ to $h = 1.5$ a substantial improvement in stability is observed. The best stability properties, however, are exhibited when the smoothing length used to weight the surface force is shorter ($h_1 = 1.0$) than that used to calculate the curvature ($h_0 = 1.5$).

Similar results were obtained using Method II (see Figure 4), with the exception that the cubic spline with $h = 1.0$ is anomalously stable. This is not completely unexpected, as it has been observed previously that SPH can be very stable for narrow ranges of relatively small smoothing lengths while more reliable numerical stability is achieved at larger smoothing lengths and by using smoother kernels [38,45,47]. Once again, the quintic spline is typically more stable than the cubic for the same parameters. The most stable set of parameters is the combination of shorter smoothing length for the surface force than that used to evaluate curvature.

Method III is unstable when used with a smoothing length of 1.5 and $\epsilon_2 = \epsilon$ (see Figure 5). The reason for this appears to be that inaccurate curvature estimates at the fringes of the interface are extrapolated throughout the computational domain. By increasing ϵ_2, only more reliable values of κ, closer to the centre of the smoothed interface, are included. Consequently, the stability of the method improves.

8.2. Equilibrium rod

Given a circle of known radius, a numerical method should reproduce the radius of curvature accurately. Once the simulation is left to run to equilibrium, the pressure within the circle should be elevated according to Equation (26).
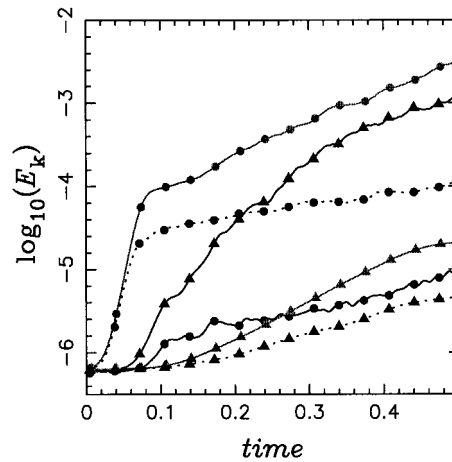
Figure 4. Evolution of $\log_{10} E_k$ with time for Method II. Curves marked with circles and triangles denote use of the cubic and quintic splines respectively. Use of $h_0 = h_1 = 1.0$, $h_0 = h_1 = 1.5$ and $h_0 = 1.5$, $h_1 = 1.0$ are denoted by black, mid-grey and dotted curves respectively.

SPH particles were set up on an initially hexagonal lattice filling a square periodic domain of width 1 unit. Particles within a circle of radius 0.25 units were given a colour of 1. All simulations used $\sigma = 1$, fluid density of 1, a sound speed of approximately 20, and a smoothing length of 1.5 times the initial nearest neighbour distance with a quintic spline kernel. For Method III, ϵ_2 was taken to be $0.25/h$. Several initial particle spacings were considered,
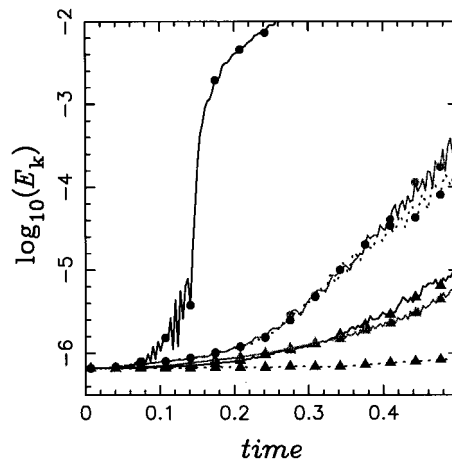

Figure 5. Evolution of $\log_{10} E_k$ with time for Method III. Curves marked with circles and triangles denote use of the cubic and quintic splines respectively. Use of $\epsilon_2 = 0.01/h$, $0.1/h$ and $0.25/h$ are denoted by black, mid-grey and dotted curves respectively.

corresponding to approximately 17, 25 and 50 particles spanning the circle. A constant small amount of viscosity was included and the simulations were run until the steady state was reached. The percentage error from the correct pressure jump ($\delta p = 4$) using each method appears in Table I. All methods achieved the correct answer to within 1 per cent when the circle was spanned by 50 particles. Methods II and III give slightly more accurate results in this test case.

8.3. Oscillating rod

A dynamic test case is the non-linear oscillation a circular droplet with an initial velocity perturbation. It is possible to consider the oscillation of initially elliptical drops, however, it can be difficult to impose the same initial state for the different methods. Since SPH uses a quasi-incompressible equation of state, it is difficult to ensure that there is no extra energy associated which the initial placement of particles. For this test case, initially circular drops were evolved to a stable steady state (see Section 8.2). The simulation was then continued with a prescribed initial velocity

$$v_x = V_0 \frac{x}{r_0} \left(1 - \frac{y^2}{r_0 r} \right) \exp(-r/r_0) \tag{40}$$

$$v_y = -V_0 \frac{y}{r_0} \left(1 - \frac{x^2}{r_0 r} \right) \exp(-r/r_0) \tag{41}$$

This velocity field is divergence free and leads to the initial cylinder of fluid being stretched out along the x-axis (for positive V_0).

Simulations were performed within the domain $0 < x < 1$ and $0 < y < 1$ using fluids of density 1 and dynamic viscosity $\mu = 0.05$. No-slip boundary conditions were applied on the domain boundaries. Results were obtained using each SPH method with a smoothing length of 1.5 times the initial nearest neighbour distance with a quintic spline kernel. For Method III, 62 was taken to be $0.25/h$. A grid-based code using the method of Youngs [26] to track the interface, flux corrected transport (FCT) to advect momenta, and a preconditioned conjugate gradient method to solve a projection equation was also applied to the problem for comparison. Similar grid-based methods have been used previously to model multiphase flows [30,40,50].

Table I. The relative error in pressure jump across the static cylinder for each method at several resolutions[a].

N_d	I (%)	II (%)	III (%)
50.0	0.8	0.04	0.1
25.0	2.2	−0.25	0.6
16.6	5.2	0.48	1.9

[a] N_d is the number of particles spanning the cylinder.

Simulations were run using $r_0 = 0.05$, $V_0 = 10$, sound speed of approximately 20, and $\sigma = 1$ for a cylinder of initial radius 0.1875. These parameters result in an initial amplitude of about 0.03 and an average velocity at the interface of about 0.8. This corresponds to a Weber number (We) of 0.24 using

$$We = \frac{\rho V^2 L}{\sigma} \tag{42}$$

where $L = 0.375$ and V are the typical length and velocity scales. The Reynolds number (Re) for this problem is approximately 6 according to

$$Re = \frac{\rho V L}{\mu} \tag{43}$$

Simulations were conducted at several resolutions using all methods. The grid-based method was found to converge with 30 cells spanning the initial cylinder. Average absolute error between the SPH methods and the converged grid-based solution as a percentage of the wave amplitude are shown in Table II. The positions of particles of colour 1 obtained using Method I at the highest resolution are shown in Figure 6. The agreement between the methods is excellent (see Figure 7).

Simulations were also run using the same parameters with $\sigma = 2$ and a sound speed of approximately 30. This corresponds to $We = 0.12$ and $Re = 6$. Average absolute error between the SPH methods and the converged grid-based solution as a percentage of the wave amplitude are shown in Table III. Once again, the agreement between the SPH methods and the grid-based solution is excellent (Figure 8).

9. DISCUSSION AND SUMMARY

Smoothed particle hydrodynamics (SPH) has been extended to simulate surface tension effects by using specialized expressions for calculating the curvature of the interface between two species of particles. The most straightforward approach (Section 5) involves calculating a corrected SPH estimate of curvature and applying it directly to obtain a surface tension force (25). While this method provides a clear framework for improving the solution by using correction factors, it does not conserve momentum exactly and the volumetric force at the

Table II. The relative error of each method at several resolutions for simulations with $We = 0.24$ and $Re = 6$[a].

N_d	I (%)	II (%)	III (%)
37.5	1.6	1.3	2.1
18.75	2.6	4.8	9.2

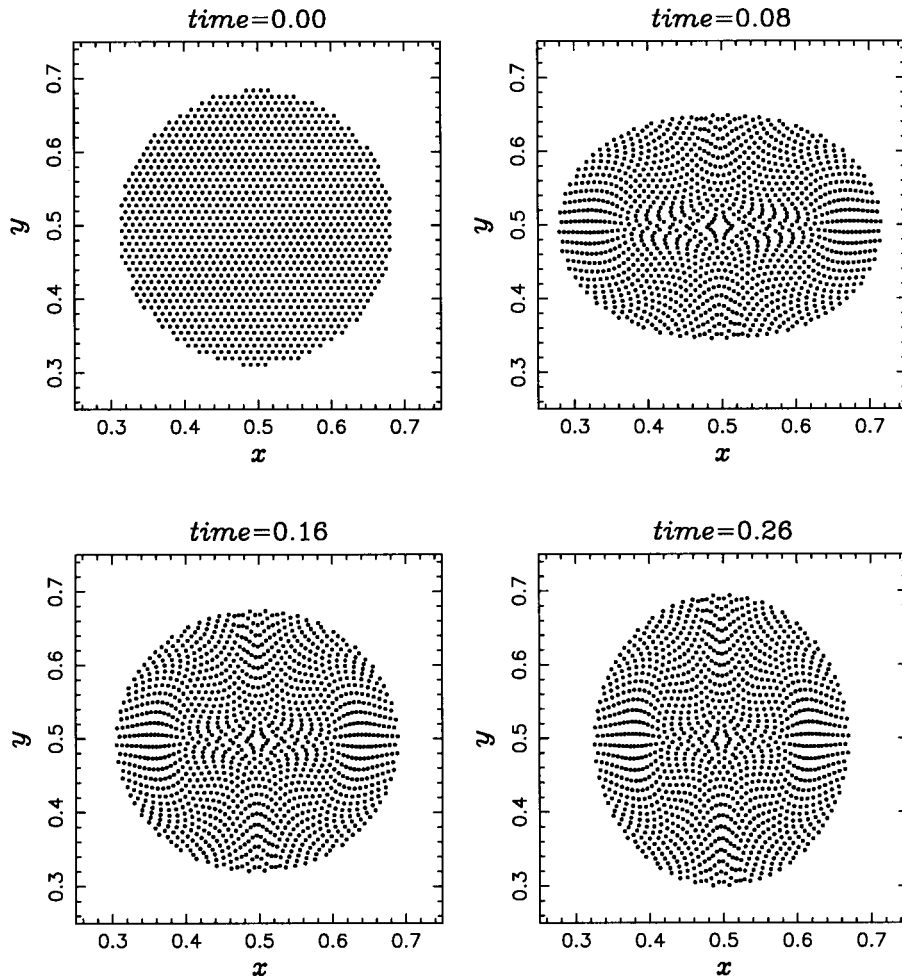[a] N_d is the number of particles spanning the initial cylinder.

Figure 6. Positions of the SPH particles of colour 1 at $t = 0.00$, 0.08, 0.16 and 0.26, using Method I with $We = 0.24$ and $Re = 6$ for the highest resolution considered.

interface becomes singular as resolution is increased. The second method presented (Section 6) employs the gradient of a stress tensor (33) to calculate surface tension, and conserves linear momentum exactly. Although not observed in this study, this approach may become unstable at high resolution. The third approach (Section 7) removes the singularity associated with the surface delta function by introducing a modified definition of pressure (38) and surface tension force (39). Despite not guaranteeing conservation of momentum, this method is expected to be most stable as resolution is increased. In addition, the removal of the singularity may allow the quasi-incompressible condition (27) to be relaxed, improving the accuracy of the method for
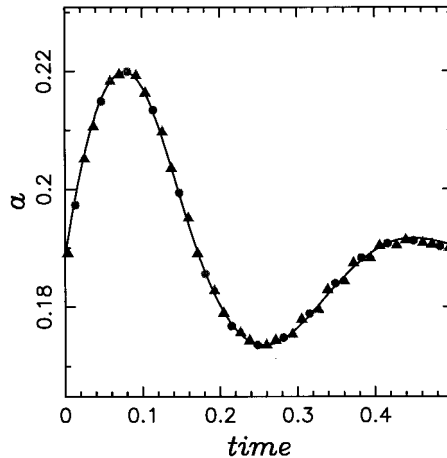
Figure 7. Semi-major axis, a, as a function of time for simulations using PLIC (solid line), Method I, Method II, and Method III (black triangle, grey circle, and grey triangles respectively) with $We = 0.24$ and $Re = 6$ for the highest resolution considered.

high surface tension coefficients. However, this technique requires extra computational expense to evaluate the gradient of the curvature. Furthermore, the third method requires the introduction of an extra parameter, $\epsilon_2 \approx 0.25/h$, to prevent instabilities resulting from errors in the curvature estimation. The appropriate method for a given problem will depend upon the relative importance of exact conservation of momentum, numerical stability, and accuracy.

A brief investigation of the stability properties of the method indicates the use of a higher-order kernel typically gives more stable results. By using a larger resolution length to calculate curvature than that used to evaluate the volumetric force, further improvements in stability were observed. However, the use of two smoothing lengths increases the computational effort. For static drop tests, all methods achieved 1 per cent accuracy with more than 50 particles spanning the droplet. Simulations of non-linear oscillations were found to be in close agreement with results obtained using a grid-based technique. All methods achieved approximately 2 per cent or better agreement with the grid-based method provided approximately 40 particles spanned the initial droplet.

Table III. The relative error of each method at several resolutions for simulations with $We = 0.12$ and $Re = 6$[a].

N_d	I (%)	II (%)	III (%)
37.5	2.0	1.8	2.1
18.75	2.9	5.5	9.9

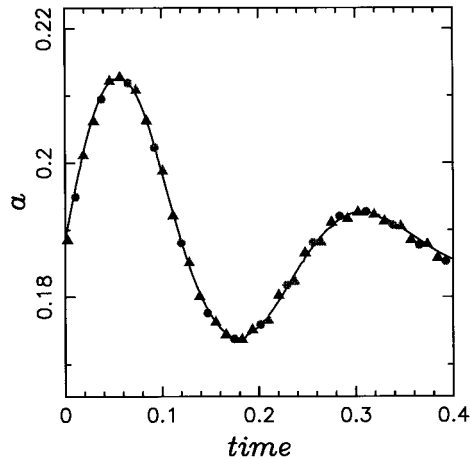[a] N_d is the number of particles spanning the initial cylinder.

Figure 8. Semi-major axis, *a*, as a function of time for simulations using PLIC (solid line), Method I, Method II, and Method III (black triangle, grey circle, and grey triangles respectively) with $We = 0.12$ and $Re = 6$ for the highest resolution considered.

The extension of the method to three-dimensional problems is, in theory, straightforward. The method could also be extended to simulations involving high-density variations. The method is currently being applied to the simulation of multiphase flow through porous media, however, the simulation of flows involving intermediate wetting fluids will require the implementation of appropriate boundary conditions at fluid–solid interfaces.

REFERENCES

1. Gingold RA, Monaghan JJ. Smoothed particle hydrodynamics: theory and application to non-spherical stars. *Monthly Notices of the Royal Astronomical Society* 1977; **181**: 375–389.
2. Lucy LB. A numerical approach to the testing of the fission hypothesis. *Astronomical Journal* 1977; **83**: 1013–1024.
3. Benz W. Smooth particle hydrodynamics: a review. In *The Numerical Modelling of Non-Linear Stellar Pulsations*, NATO Workshop, Buchler JR (ed.). Les Arcs: France, 1989; 269.
4. Monaghan JJ. Smoothed particle hydrodynamics. *Annual Review of Astronomy and Astrophysics* 1992; **30**: 543–574.
5. Randles PW, Libersky LD. Smooth particle hydrodynamics: some recent improvements and applications. *Computer Methods in Applied Mechanics and Engineering* 1996; **139**: 375–408.
6. Monaghan JJ. Simulating free surface flows with SPH. *Journal of Computational Physics* 1994; **110**: 399–406.

7. Morris JP, Fox PJ, Zhu Y. Modeling low Reynolds number incompressible flows using SPH. *Journal of Computational Physics* 1997; **136**: 214–226.
8. Zhu Y, Fox PJ, Morris JP. Smoothed particle hydrodynamics model for flow through porous media. In *Proceedings of The 9th International Conference of the Association for Computer Methods and Advances in Geomechanics*, China, vol. 2, Yuan Jian-Xin (ed.). AA Balkema, 1997; 1041–1046.
9. Zhu Y, Fox PJ, Morris JP. A pore-scale numerical model for flow through porous media. *International Journal for Numerical and Analytical Methods in Geomechanics* 1999; **23**: 881–904.
10. Hunter JP. Surface tension in smoothed particle hydrodynamics. Honours thesis, Mathematics Department, Monash University, Melbourne, Australia, 1992.
11. Monaghan JJ. An SPH formulation of surface tension. Applied Mathematics Reports and Preprints, Monash University (95/44), 1995.
12. Tsai W, Yue DKP. Computation of nonlinear free-surface flows. *Annual Review of Fluid Mechanics* 1996; **28**: 249–278.
13. Fukai J, Zhao Z, Poulikakos D, Megaridis CM, Miyatake O. Modeling of the deformation of a liquid droplet impinging upon a flat surface. *Physics of Fluids A* 1993; **5**(11): 2588–2599.
14. Szabo P, Hassager O. Simulation of free surfaces in 3D with the arbitrary Lagrange/Euler method. *International Journal for Numerical Methods in Engineering* 1995; **38**: 717–734.
15. Mashayek F, Ashgriz N. A spine-flux method for simulating free surface flows. *Journal of Computational Physics* 1995; **122**: 367–379.
16. Thomas TG, Leslie DC, Williams JJR. Free surface simulations using a conservative 3D code. *Journal of Computational Physics* 1995; **116**: 52–68.
17. Rider WJ, Kothe DB. Stretching and tearing interface tracking methods. AIAA Paper 95-1717, 1995.
18. Medale M, Jaeger M. Numerical simulation of incompressible flows with moving interfaces. *International Journal for Numerical Methods in Fluids* 1997; **24**: 615–638.
19. Rudman MJ. Volume tracking methods for interfacial flow calculations. *International Journal for Numerical Methods in Fluids* 1997; **24**: 671–691.
20. Scardovelli R, Zaleski S. Direct numerical simulation of free-surface and interfacial flow. *Annual Review of Fluid Mechanics* 1999; **31**: 567–603.
21. Colella P, Woodward PR. The piecewise-parabolic method (PPM) for gas dynamical simulations. *Journal of Computational Physics* 1984; **54**: 174–201.
22. Sethian JA. *Level Set Methods: Evolving Interfaces in Geometry*, *Fluid Mechanics, Computer Vision, and Materials Science*. Cambridge University Press: Cambridge, 1996.
23. Sussman M, Smereka P, Osher S. A level set approach for computing solutions to incompressible two-phase flow. *Journal of Computational Physics* 1994; **114**: 146–159.
24. Noh WF, Woodward P. SLIC (simple line interface calculation). In *Lecture Notes in Physics*, vol. 59, van Dooren AI, Zandbergen PJ (eds). Springer: New York, 1976; 330–340.
25. Hirt CW, Nichols BD. Volume of fluid (VOF) methods for the dynamics of free boundaries. *Journal of Computational Physics* 1981; **39**: 201–225.
26. Youngs DL. Time-dependent, multi-material flow with large fluid distortion. In *Numerical Methods for Fluid Dynamics*, Morton KW, Baines MJ (eds). Academic: New York, 1982; 273–285.
27. Glimm J, McBryan O, Menikoff R, Sharp DH. Front tracking applied to Rayleigh–Taylor instability. *SIAM Journal on Science and Statistics in Computing* 1986; **7**: 230–251.
28. Tryggvason G, Unverdi SO. Computations of three-dimensional Rayleigh–Taylor instability. *Physics of Fluids A* 1990; **2**: 656–659.
29. Udaykumar HS, Kan H-C, Shyy W, Tran-Son-Tay R. Multiphase dynamics in arbitrary geometries on fixed Cartesian grids. *Journal of Computational Physics* 1997; **137**: 366–405.
30. Rider WJ, Kothe DB, Mosso SJ, Cerutti JH, Hochstein JI. Accurate solution algorithms for incompressible multiphase flows. AIAA Paper 95-0699, 1995.
31. Brackbill JU, Kothe DB, Zemach C. A continuum method for modelling surface tension. *Journal of Computational Physics* 1992; **100**: 335–354.
32. Kothe DB, Mjolsness RC. RIPPLE: A new model for incompressible flows with free surfaces. *AIAA Journal* 1992; **30**(11): 2694–2700.
33. Richards JR, Lenhoff AM, Beris AN. Dynamic breakup of liquid-liquid jets. *Physics of Fluids* 1994; **6**: 2640–2655.
34. Le Veque RJ, Li Z. The immersed interface method for elliptic equations with discontinuous coefficients and singular sources. *SIAM Journal on Numerical Analysis* 1994; **31**: 1019–1044.
35. Weatherburn CE. On differential invariants in geometry of surfaces, with some applications to mathematical physics. *Quarterly Journal of Mathematics* 1927; **50**: 230–269.

36. Schoenberg IJ. Contributions to the problem of approximation of equidistant data by analytic functions. *Quarterly Journal of Applied Mathematics* 1946; **4**: 45.
37. Courant R, Friedrichs K, Lewy H. Über die partiellen differenzengleichungen der mathematischen physik. *Mathematische Annalen* 1928; **100**: 32–74.
38. Morris JP. Analysis of SPH with applications. PhD thesis, Mathematics Department, Monash University, Melbourne, Australia, 1996.
39. Aleinov I, Puckett EG. Computing surface tension with high-order kernels. In *Proceedings of The 6th International Symposium of Computational Dynamics, Lake Tahoe, CA*, September, Oshima K (ed.), 1995; 13–18.
40. Rudman MJ. A volume-tracking method for incompressible multifluid flows with large density variations. *International Journal for Numerical Methods in Fluids* 1998; **28**: 357–378.
41. Belytschko T, Krongauz Y, Organ D, Flemming M, Krysl P. Meshless methods: an overview and recent developments. *Computer Methods in Applied Mechanics and Engineering* 1996; **139**: 3–47.
42. Lafaurie B, Nardone C, Scardovelli R, Zaleski S, Zanetti G. Modeling merging and fragmentation in multiphase flows with SURFER. *Journal of Computational Physics* 1994; **113**: 134–147.
43. Swegle JW, Hicks DL, Attaway SW. Smoothed particle hydrodynamics stability analysis. *Journal of Computational Physics* 1995; **116**: 123–134.
44. Phillips GJ, Monaghan JJ. A numerical method for 3-dimensional simulations of collapsing, isothermal, magnetic gas clouds. *Monthly Notices of the Royal Astronomical Society* 1985; **216**: 883–895.
45. Morris JP. A study of the stability properties of SPH. Applied Mathematics Reports and Preprints, Monash University (94/22), 1994.
46. Balsara DS. Von-Neumann stability analysis of smoothed particle hydrodynamics—suggestions for optimal algorithms. *Journal of Computational Physics* 1995; **121**: 357–372.
47. Morris JP. A study of the stability properties of SPH. *Publications of the Astronomical Society of Australia* 1996; **13**: 97–102.
48. Brookshaw L. A method of calculating radiative heat diffusion in particle simulations. *Proceedings of the Astronomical Society of Australia* 1985; **6**: 207–210.
49. Sussman M, Almgren A, Bell J, Colella P, Howell L, Welcome M. An adaptive level set approach for incompressible two-phase flows. *Journal of Computational Physics* 1999; **148**: 81–124.
50. Rider WJ, Kothe DB, Puckett EG, Aleinov ID. Accurate and robust methods for variable density incompressible flows with discontinuities. In *Proceedings of the Workshop on Barriers and Challenges in CFD, Langely, VA*, August, Venkatakrishnan V, Salas MD, Chakravarthy SR (eds), 1996; 213–230.